Electronic Supplementary Information (ESI)

Formation Mechanisms of Hollow Manganese Hexacyanoferrate Particles and Construction of Multiple-Shell Structure

Fumiyuki Shiba,*[a] Asumi Yamamoto,[b] Yuuki Shinta,[c] Ushio Mameuda,[a] Yuuki Tahara,[c] and Yusuke Okawa[a]

[a] Department of Materials Science, Graduate School of Engineering, Chiba University

[b] Department of Image and Materials Science, Graduate School of Advanced Integration Science, Chiba University

[c] Department of Image Science, Faculty of Engineering, Chiba University

1-33 Yayoicho, Inageku, Chiba 263-8522, Japan

*E-mail: shiba@faculty.chiba-u.jp

Estimation of the elemental composition using the TEM-EDX method

The elemental compositions of the Mn-HCF particles were evaluated by the TEM-EDX method. Fig. S1 shows EDX spectra for the as-prepared and hollow Mn-HCF particles shown in Fig. 3 (reaction time 40 min). The spectra seem to be similar and indicate both the Mn-HCF particles contain K^+ as the component. Note that the Al and Cu signals are from the TEM specimen holder and the specimen's TEM grid, respectively.

Fig. S2 indicates the atomic compositions of K and Mn, relative to Fe, at different reaction times: the mean valence of Fe is calculated based on the charge balance in the particles. The Mn/Fe and K/Fe ratios were roughly 1.1 and 1.5, respectively. The former slightly decreased with reaction time, whereas the latter tended to increase. Moreover, both the ratios were larger for the hollow particles than for the as-prepared ones; the differences in the compositional ratios between the as-prepared and hollow particles decreased with reaction time. The estimated mean Fe valence suggests $[Fe^{II}(CN)_6]^{4-}$ and $[Fe^{III}(CN)_6]^{3-}$ are coprecipitated with Mn^{2+}.

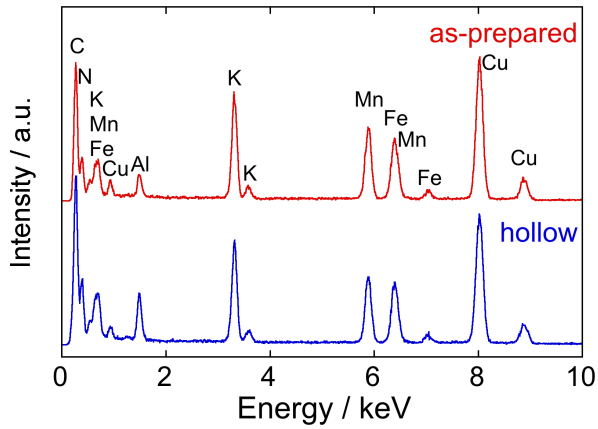

Fig. S1 TEM-EDX spectra for the Mn-HCF particles in Fig. 3 (at 40 min), where the Al and Cu signals are from the specimen holder of the TEM and the TEM grid of the specimen, respectively.

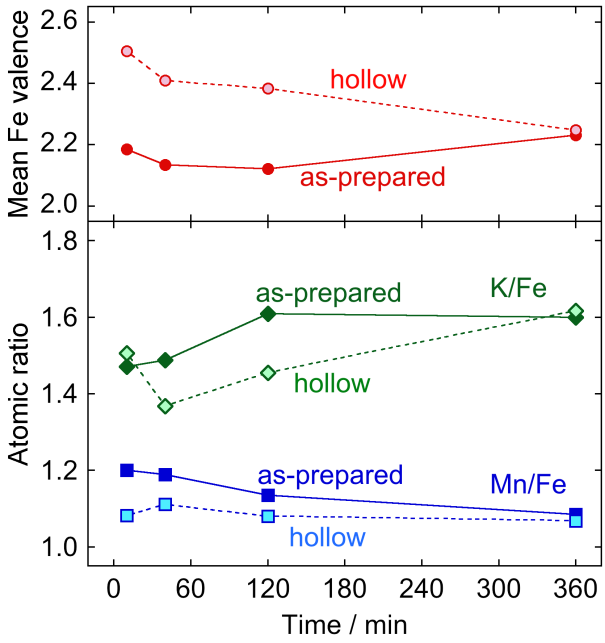

Fig. S2 Atomic compositions of K and Mn, relative to Fe, at different reaction times estimated by the EDX measurement. The mean Fe valences are calculated based on the charge balance relationships among K^+, Mn^{2+}, and $[Fe(CN)_6]^{3-/4-}$ ions using the atomic ratios.

Atomic absorption spectrometry for the estimation of Mn^{2+} and $[Fe(CN)_6]^{3-}$ concentrations in the aqueous phase

Atomic absorption (AA) spectrometry was employed to measure the Mn^{2+} and $[Fe(CN)_6]^{3-}$ concentrations in the aqueous phase (Varian SpectrA55, C_2H_2/air flame). For evaluating the formation process (Fig. 4b), the supernatant solution was separated from the reacting sol by removing the precipitate with a syringe filter (pore size 0.22 μm). The supernatant solution (4 mL) was mixed with 1 mL EDTA solution (0.2 mol/L EDTA-2Na + 0.2 mol/L NaOH) to prevent further precipitation, and diluted to 20 mL with distilled water. The AA absorbance was measured at 403.1 nm and 372.0 nm for Mn and Fe, respectively. For the solubility estimations, the freeze-dried particles were dispersed in distilled water (~30 mL) and kept at 25 °C for 30 min with magnetic stirring. Then the supernatant solution was obtained using the syringe filter. After diluting to 1/2 with distilled water, Mn^{2+} content was measured at 279.5 nm. The different wavelengths were used to fit the sensitivity to the concentration ranges of the samples.

Calculation of free Mn^{2+} ion concentration in the presence of citrate ions

The free Mn^{2+} concentration, $[Mn^{2+}]$, in the reacting sol is formulated with the equilibrium constants and the mass-balance equations. When the reaction pH is higher than the citric acid's pK_{a3}, the contributions of H_3L and H_2L^- species may be omitted in the calculation, where L^{3-} denotes citrate ion (the reaction pH 6.44 whereas pK_{a3} 5.69). Hence, the equilibrium relationships and the corresponding equilibrium constants

$$HL^{2-} \rightleftharpoons H^+ + L^{3-} \qquad K_{a3} = [H^+][L^{3-}]/[HL^{2-}]$$
$$Mn^{2+} + HL^{2-} \rightleftharpoons MnHL \qquad \beta_{MHL} = [MnHL]/[Mn^{2+}][HL^{2-}]$$
$$Mn^{2+} + L^{3-} \rightleftharpoons MnL^- \qquad \beta_{ML} = [MnL^-]/[Mn^{2+}][L^{3-}]$$

should be considered for the formulation. The following mass-balance equations

$$C_{Mn} = [Mn^{2+}] + [MnHL] + [MnL^-]$$
$$C_L = [HL^{2-}] + [L^{3-}] + [MnHL] + [MnL^-]$$

stand, where C_{Mn} and C_L denote the total concentrations for the Mn^{2+} and L^{3-} species, respectively. Combining the equations, one obtains

$$(\beta_{MHL}[H^+] + \beta_{ML}K_{a3})[Mn^{2+}]^2 + \{(\beta_{MHL}[H^+] + \beta_{ML}K_{a3})(C_L - C_{Mn}) + ([H^+] + K_{a3})\}[Mn^{2+}] - ([H^+] + K_{a3})C_{Mn} = 0.$$

Solving this equation with given $[H^+]$, C_{Mn}, and C_L values, one obtains $[Mn^{2+}]$ value at the condition. On estimating $[Mn^{2+}]$ values, $[H^+] = 10^{-6.44}$ mol/L and $C_L = 0.02$ mol/L were used from the reaction pH 6.44 and the Na_3-Cit concentration, respectively. The data in Fig. 4b was used for the C_{Mn} value at the respective reaction time.

Stability of free $[Fe(CN)_6]^{3-}$ ion in sodium citrate aqueous solution

The free $[Fe(CN)_6]^{3-}$ ion concentration in a sodium citrate aqueous solution was monitored with absorbance at 420 nm to verify whether free citrate ion could reduce free $[Fe(CN)_6]^{3-}$ ion in the absence of Mn^{2+} ion. As shown in the inset of Fig. S3, the spectra for $K_3[Fe(CN)_6]$ (0.01 mol/L) has an absorption maxima at 420 nm ($\varepsilon = 1.0 \times 10^3$ L mol^{-1} cm^{-1}), but that for $K_4[Fe(CN)_6]$ has no absorption at this wavelength. Hence the absorbance decrease at 420 nm, if it occurs, is attributed to the reduction of $[Fe(CN)_6]^{3-}$ ion.

The Na_3-Cit aqueous solution was prepared by dissolving 1 mmol Na_3-Cit in 45 mL distilled water. Being kept the temperature at 25 °C in a water bath, 5 mL $K_3[Fe(CN)_6]$ aqueous solution (0.05 mol/L) was added to the citrate aqueous solution under magnetic stirring. The molar concentrations of Na_3-Cit and $K_3[Fe(CN)_6]$ were the same as the Mn-HCF preparation condition after the mixing. On the absorbance measurement, 4 mL of the solution was diluted to 20 mL with distilled water. Thus the total $[Fe(CN)_6]^{3-/4-}$ concentration on the absorbance measurement was 1 mmol/L. As shown in Fig. S3, the absorbance was unchanged with time, meaning free $[Fe(CN)_6]^{3-}$ ion is stable and not reduced in the sodium citrate aqueous solution in the absence of Mn^{2+} ion. Therefore, it is reasonable to consider that $[Fe(CN)_6]^{3-}$ ions are reduced by Mn^{2+}-citrate complex, rather than free citrate ions, during the present precipitation process.

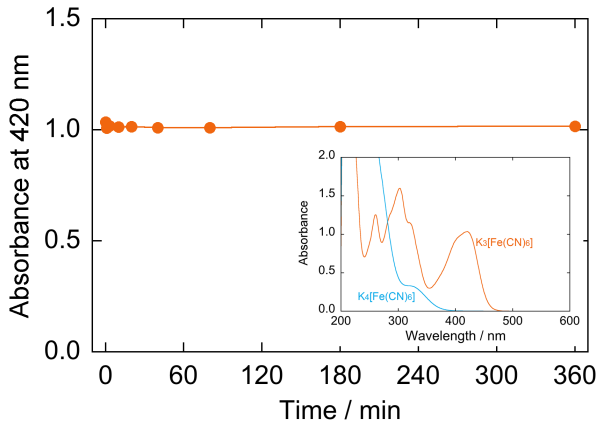

Fig. S3 Absorbance at 420 nm of $K_3[Fe(CN)_6]$ aqueous solution with sodium citrate as a function of time. The inset shows the absorption spectra $K_3[Fe(CN)_6]$ and $K_4[Fe(CN)_6]$ aqueous solutions (1 mmol/L).

Particles precipitating from the supernatant solution after removing the Mn-HCF particles

As shown in Fig. 4, the shell-part of the as-prepared particle grew even at 360 min. This implies the aqueous phase was still in a supersaturated condition to the monoclinic Mn-HCF phase. In fact, monoclinic Mn-HCF particles precipitated in the supernatant solution that had been separated from the reacting sol by removing the Mn-HCF particles (Fig. S4). That is, a Mn-HCF sol was prepared in the same condition for Fig. 3. A transparent supernatant solution was obtained from the sol at 40 min by removing the Mn-HCF particles with a syringe filter (pore size 0.22 μm). The supernatant solution was then placed in a water bath to keep at 25 °C for 320 min under magnetic stirring; its turbidity slowly increased with time. The formed precipitate was collected by suction filtration and rinsed with distilled water.

The XRD pattern in Fig. S4a matches with the monoclinic Mn-HCF (PDF 01-089-8979). The characteristic $\bar{2}02$ and 202 reflections for the monoclinic Mn-HCF are clearly observed. The FE-SEM image in Fig. S4b indicated that the particles are basically platelet, but some seem to be twin particles. Fig. S4c shows the SAED pattern from a single particle in the inset; the Laue spots are indexed to the reflections from the monoclinic Mn-HCF with the [001] incident direction.

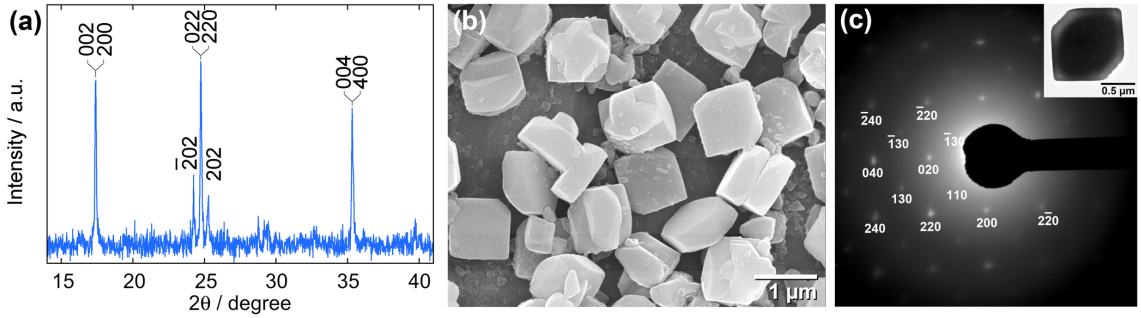

Fig. S4 Particles precipitated from the supernatant solution separated from the Mn-HCF particles at 40 min of the reaction. (a) XRD pattern using Cu Kα radiation (λ = 1.5418 Å), (b) FE-SEM image, and (c) SAED pattern from the single particle in the inset.

SEM observation of a cracked double-shell hollow particle

To indicate the matryoshka-like structure for the multiple-shell hollow particles, an FE-SEM image of a cracked double-shell hollow particle is shown in Fig. S5. A shell surrounds an inner hollow particle; there is a space between them.

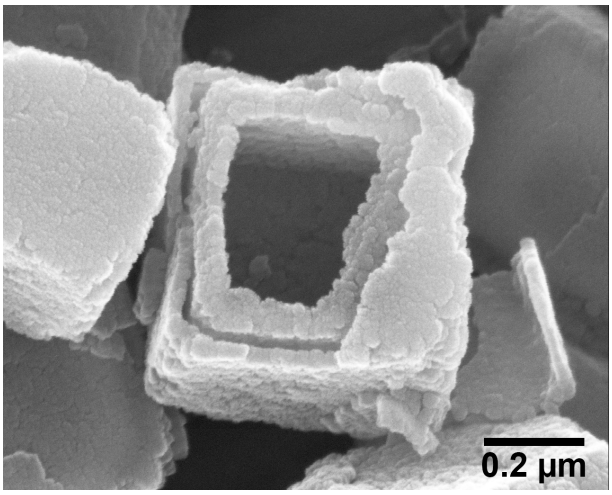

Fig. S5 FE-SEM image of a cracked double-shell hollow Mn-HCF particles.

Influence of agglomeration of the seed particles on the multiple-shell hollow particles construction

The present procedure for the multiple-shell structure construction includes a solid-liquid separation process using suction filtration. As these processes could cause agglomeration among the particles, gelatin was employed to protect the particles from the suction pressure during the separation process. Adding gelatin before the separation process appears to improve the seed particles' dispersity, although it might not be perfect. Gelatin did not relate to the hollow structure formation. However, gelatin tended to broaden the size distribution for the single-shell hollow particles by affecting the nucleation stage if it existed at the start of the reaction. Hence the gelatin solution was added at the middle of each growth step for the multiple-shell construction (Fig. S6).

In the present procedure, the multiple-shell hollow particles are prepared based on the additional growth technique. If some seed particles are in touch with each other at the additional growth step, they would be wrapped by an additional layer together. The additional layer is converted to the outer shell by the washing process, resulting in two-in-one (or three-in-one, etc.) multiple-shell hollow particles, as shown in Fig. S7. This situation occurred more frequently when gelatin was not added before the separation process. Although these

kinds of particles might include other kinds of interests, their formation would broaden the size and structural distribution, especially when repeating the additional growth process to construct triple- or quadruple-shell particles.

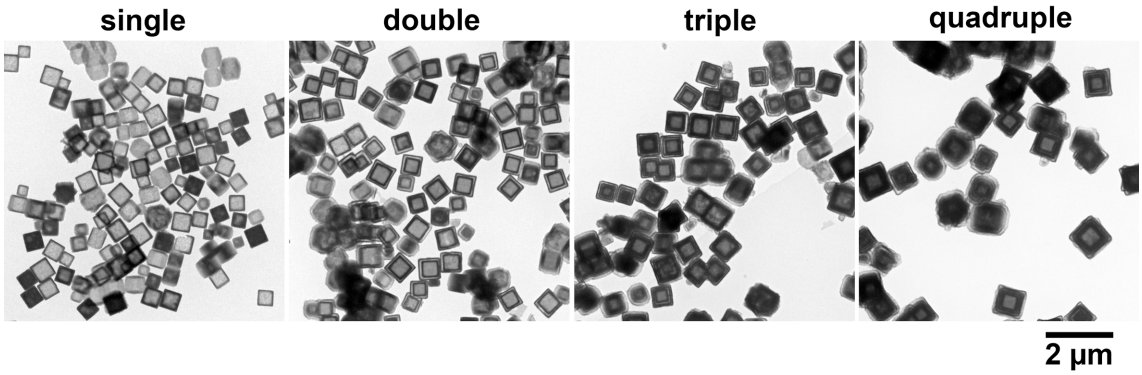

Fig. S6 Single- and multiple-shell hollow Mn-HCF particles prepared with the additional growth procedure by adding a small amount of gelatin before the solid-liquid separation process.

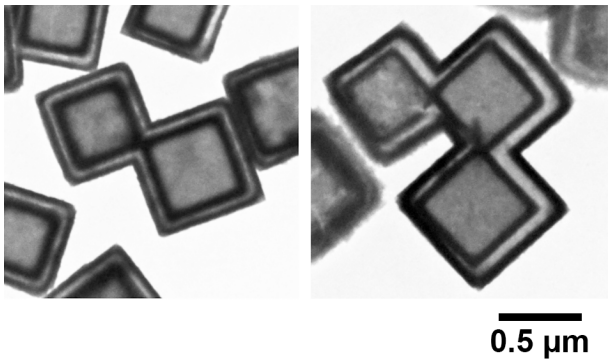

Fig. S7 Two-in-one and three-in-one double-shell hollow Mn-HCF particles that contain contacted seed particles in them.